Chinese Chemical Letters 33 (2022) 3792–3796

Contents lists available at ScienceDirect

Chinese Chemical Letters

journal homepage: www.elsevier.com/locate/cclet

Heterojunction architecture of Nb_2O_5/g-C_3N_4 for enhancing photocatalytic activity to degrade organic pollutants and deactivate bacteria in water

Xudong Yang[a], Jun Duan[b], Xian Zhang[a], Hongyu Zhang[a], Xinlei Liu[a], Yueqi Feng[a], Maosheng Zheng[a,*]

[a] The Key Laboratory of Resources and Environmental System Optimization, Ministry of Education, College of Environmental Science and Engineering, North China Electric Power University, Beijing 102206, China
[b] The Key Laboratory of Water and Sediment Science, Ministry of Education, College of Environment Science and Engineering, Peking University, Beijing 100871, China

ARTICLE INFO

Article history:
Received 19 August 2021
Revised 27 September 2021
Accepted 7 November 2021
Available online 12 November 2021

Keywords:
Graphitic carbon nitride
Niobium pentoxide
Photocatalysis
Escherichia coli disinfection
Dyes removal

ABSTRACT

Water pollution has become a serious problem owing to the development of society. Photocatalysis is a promising approach to remove various pollutants in water, such as organic pollutants and antibiotic resistance bacteria. Meanwhile, the design of heterojunction between two semiconductors is an effective path to improve photocatalytic properties due to its potential in improving separation and transfer of photoinduced carriers. In this study, Nb_2O_5/g-C_3N_4 (NO/CN) composite materials were prepared through a one-step heating method. Characterizations confirmed successful preparation of NO/CN heterojunction structure and better optical properties than pure g-C_3N_4 and Nb_2O_5. NO/CN composite materials showed excellent photocatalytic efficiency for *Escherichia coli* (*E. coli*) inactivation (95%) compared with the pure Nb_2O_5 (10%) and g-C_3N_4 (77%). Meanwhile, NO/CN exhibited better organic pollutants removal (RhB for 94%, methyl orange (MO) for 15% and methylene blue (MB) for 87%) under visible light, which is likely owing to the heterojunction structure between g-C_3N_4 and Nb_2O_5 that leads to the good separation of photogenerated electron-hole pair. Free radical scavenging and electron spin resonance (ESR) experiments demonstrated that superoxide radicals ($^{\bullet}O_2^-$) and holes (h^+) were the dominant radicals. Therefore, the NO/CN was proposed to be a promising material for effective disinfection and removal of organic contaminants in water treatment.

The rapid development of economy and industries of modern society have caused serious water pollution, which impacts the human health and economy growth [1]. World Health Organization (WHO) reported millions of people death due to the pathogens related disease in uncleaned drinking water, *i.e., Escherichia coli* (*E. coli*) [2]. Such pathogens have become increasingly resistant to the conventional disinfection chemicals and methods, so the disinfection efficiencies have been largely weakened [3–5], and the inadequate disinfection of drinking water may cause more health issue of human or even death [6]. Moreover, a large number of persistent and toxic chemicals are produced and used worldwide every year, such as dyes and pharmaceuticals, which also show low treatment efficiencies by conventional wastewater treatment plants (WWTPs) [7–9]. Thus, it is quite urgent to find more advanced approaches to conquer these water pollution problems.

As an environmentally friendly and energy-saving technology, photocatalysis has attracted great interests of researchers for the advanced disinfection and removal of organic chemicals, owing to the usage of clean and renewable solar energy and the formation of reactive oxygen species (ROSs) [10–12]. Under light, the generated of photoinduced electrons (e^-) and holes (h^+) can interact with dissolved O_2 and H_2O to form ROSs such as superoxide radicals ($^{\bullet}O_2^-$) and hydroxyl radicals ($^{\bullet}OH$) [13]. Subsequently, these ROSs will attack the bacteria and organic pollutant molecules and show improved removal efficiencies [14].

Graphitic carbon nitride (g-C_3N_4) has been proved to be a promising photocatalyst for water treatment with a moderate band gap (2.7 eV) and favorable light absorption (wavelength < 460 nm) [15]. The existence of strong C-N bond in the structure makes the g-C_3N_4 chemically stable and easy to synthesis [16]. However, the

* Corresponding author.
E-mail address: maoshengzheng@ncepu.edu.cn (M. Zheng).

https://doi.org/10.1016/j.cclet.2021.11.031
1001-8417/

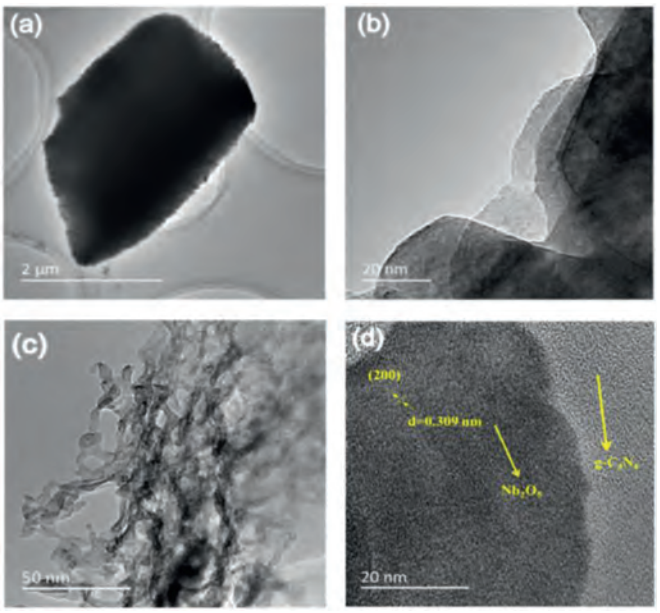

Fig. 1. TEM (a) and HRTEM (b) images of pure g-C_3N_4. TEM (c) and HRTEM (d) images of Nb_2O_5/g-C_3N_4.

application of bare g-C_3N_4 in pollutant degradation is full of limitation because of the rapid recombination of e^- and h^+ pairs, which will cause low quantum efficiency [17,18]. Thus, it is necessary to seek for other ways to solve these questions. Constructing photocatalyst heterojunction is a positive method to enhance the photocatalytic activity owing to the effective separation of photoinduced e^- and h^+ [19]. Niobium pentoxide (Nb_2O_5) is a good n-type transition metal oxide semiconductor and has been coupled with various photocatalysts to enhance the photocatalytic performance [20]. For instance, titanium oxide (TiO_2) was coupled with Nb_2O_5 to form heterojunctions, which intensively enhanced photocatalytic activity for α-phenethyl alcohol and the observed rate constant (k_{obs}) was increased by 3 or 8 folds compared to that of rutile TiO_2 and Nb_2O_5, separately [21]. Moreover, the charge band edge (E_{CB}) and valence band edge (E_{VB}) of Nb_2O_5 ($E_{CB} = -0.9$ eV, $E_{VB} = 2.5$ eV) could enable it to match with g-C_3N_4 ($E_{CB} = -1.13$ eV, $E_{VB} = 1.57$ eV) to establish the heterojunction structure [22], which can dramatically facilitate the charge carrier separation and enhance overall photocatalytic performance [23].

Herein, a novel Nb_2O_5/g-C_3N_4 (NO/CN) heterojunction photocatalysts were synthesized and a series of characterizations were conducted to investigate its various properties. Besides, the photocatalytic ability of the NO/CN materials is investigated by using *E. coli*, and certain contaminants such as rhodamine B (RhB), methylene blue (MB), methyl orange (MO). Besides, free radical capture and electron spin resonance (ESR) experiments have shown that $^{\bullet}O_2^-$ and h^+ are the key free radicals. Finally, the possible reaction mechanism was proposed. In summary, this study has theoretical and practical significance in the disinfection process and water treatment, and the elucidation of photocatalytic mechanism. Additionally, experimental details are exhibited in Texts S1-5 in Supplementary information.

The morphologies of original g-C_3N_4 and NO/CN materials were considered *via* Transmission electron microscopy (TEM) and high-resolution TEM (HRTEM), which are illustrated in Fig. 1. g-C_3N_4 displays the sheet structure, which can both reduce the diffused distance of photoinduced charge carriers [24] and offer abundant surface sites to support the Nb_2O_5 nanoparticles (Figs. 1a and b). As can be seen in Fig. 1c, on the surface of g-C_3N_4, nanoscale Nb_2O_5 particles were dispersed with a chain-like structure. The lattice fringe space of Nb_2O_5 was measured to be 0.309 nm in Fig. 1d, corresponding to the (200) plane of Nb_2O_5 [25]. It is pretty clear to observe the border of g-C_3N_4 and Nb_2O_5, suggesting that Nb_2O_5 has been successfully patched on g-C_3N_4. In addition, the energy dispersive X-ray spectroscopy (EDS) and elemental mapping results of NO/CN proved the evenly distributed C, N, O, and Nb elements in the composite materials (Figs. S1 and S2 in Supporting information).

Powder X-ray diffraction (XRD) characterizations were utilized to measure the phase structure and crystallinity of NO/CN material. As shown in Fig. 2a, pure g-C_3N_4 holds two characteristic peaks at 13.1° and 27.4°, which are attributed to the periodic stacking of tri-*s*-triazine rings in plane (100) and graphitic layers (002), respectively [26]. Besides, the peaks of Nb_2O_5 are matched with orthorhombic phase of Nb_2O_5 (JCPDS No. 19-0862). The NO/CN composite materials barely revealed the characteristic peaks of Nb_2O_5, which may be attributed to the low content of Nb_2O_5 and excellent dispersion of Nb_2O_5 on the g-C_3N_4 [24]. Additionally, the peaks of g-C_3N_4 became weak and there is no impurity peak in the NO/CN material, which illustrate that NO/CN has been combined successfully.

X-ray photoelectron spectroscopy (XPS) was recorded to verify the elemental component and valent state of composite material. The NO/CN consists of element C, N, Nb, and O according to the survey spectra (Fig. 2b), which suggests the heterojunction formed between g-C_3N_4 and Nb_2O_5. In Fig. 2c, two significant peaks of C 1s were located at 288.0 eV and 284.8 eV, which can be associated with C–C single bond and the double bond between carbon atoms and nitrogen atoms [27]. The high-resolution N 1s spectra (Fig. 2d) exhibits three obvious peaks centered at 398.5 eV, 400.0 eV and 404.3 eV, which can be assigned to sp^2-hybridized N (C=N-C), pyrrolic N and π-excitation, respectively [28,29]. In the high-resolution Nb 3d spectra (Fig. 2e), two apparent peaks located at 206.9 eV and 209.6 eV were attributed to the Nb $3d_{3/2}$ and Nb $3d_{5/2}$ levels, which was consistent with previous researches of Nb_2O_5 [30]. Finally, based on Fig. 2f, the high-resolution spectra of O 1s at 532.9 eV are attributed to the lattice oxygen of Nb_2O_5.

The optical properties of the NO/CN are studied *via* employing the UV-vis diffused reflectance spectra (UV-DRS). In Fig. 3a, g-C_3N_4 and Nb_2O_5 possess the light absorption edge of roughly 440 and 395 nm, respectively, corresponding to the band gap of 2.82 eV and 3.14 eV based on Fig. 3b [31]. The light absorption edge of NO/CN composite exhibited a slight red shift from 440 nm to 449 nm, which indicates that the band gap of NO/CN composite is narrowed (2.76 eV) and can efficiently utilize visible light. Additionally, the band structures of g-C_3N_4, Nb_2O_5 and NO/CN are further analyzed by using valence band XPS in Fig. 3c, which were 1.73, 2.67 and 1.94 eV, respectively. According to the results of UV-DRS and VB-XPS, the diagrammatic sketch of band structure of g-C_3N_4, and NO/CN were depicted in Fig. 3d. Compared with g-C_3N_4, the VB and CB position of NO/CN were altered after loading Nb_2O_5, which indicates that the obtained heterojunction structure would benefit the photocatalytic activity.

Then, the photocatalytic experiments were performed to examine the disinfection ability of the as-prepared photocatalysts. As observed in Fig. 4a, the amount of viable cells remain nearly unchanged under visible light irritation within 240 min and only 0.7 log CFU/mL of cells were inactivated with the addition of pure Nb_2O_5, indicating visible light and pure Nb_2O_5 have limited impact on *E. coli* inactivation. In the presence of pure g-C_3N_4, 5.4 log CFU/mL of cells were disinfected within 240 min, showing the good visible light responses of g-C_3N_4. The disinfection efficiency was further enhanced in the presence of NO/CN composite material, with 6.67 log CFU/mL of cells disinfected within 240 min. The different disinfection ability of various materials could also be clearly observed in the final bacterial colony counts (Fig. S3 in Sup-

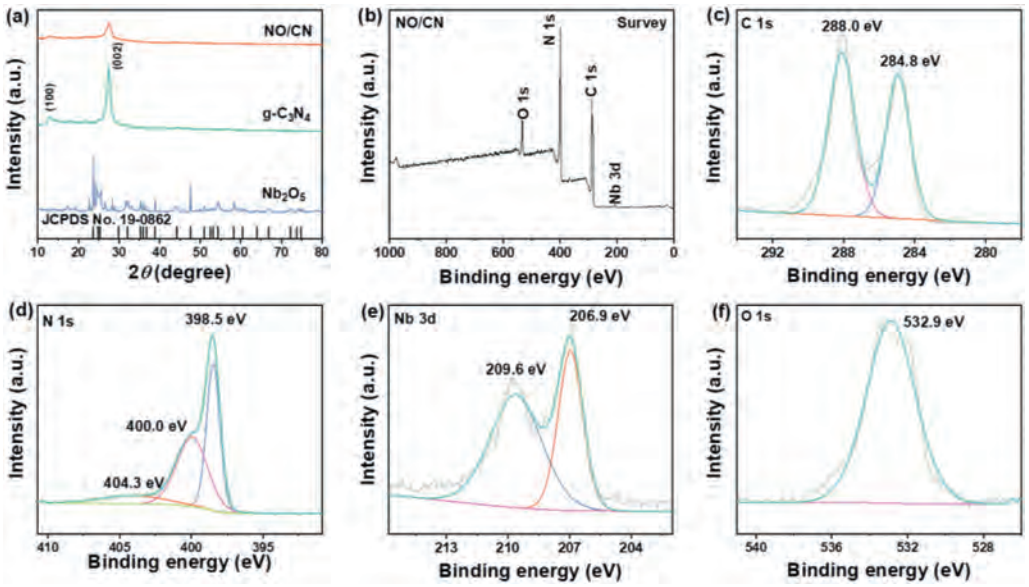

Fig. 2. (a) XRD patterns of g-C_3N_4, Nb_2O_5, and NO/CN; (b) XPS survey spectra for NO/CN composite; (c-f) the high-resolution spectra of C 1s, N 1s, Nb 3d, and O 1s for NO/CN composite.

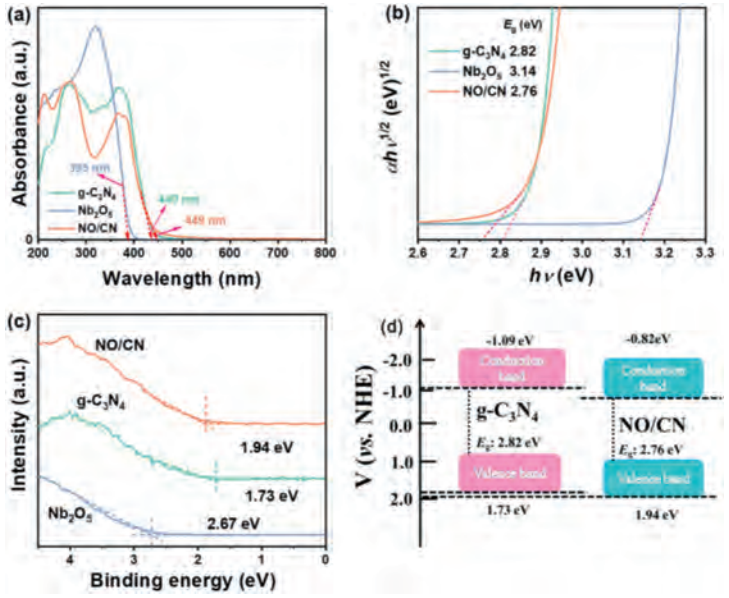

Fig. 3. (a) UV-DRS, (b) plots of the $(\alpha h\nu)^{1/2}$ *vs.* photon energy ($h\nu$), and (c) VB-XPS of pure g-C_3N_4, Nb_2O_5, and NO/CN. (d) Schematic band structure of g-C_3N_4 and NO/CN.

porting information). Apparently, the NO/CN heterojunction photocatalyst has improved photocatalytic sterilization activity than pristine Nb_2O_5 and g-C_3N_4, which can be caused by the construction of heterojunction structure and better separation of charge carriers that promotes the generation of ROSs. Meanwhile, potassium ion (K^+) was a crucial intracellular ion that can regulate protein synthesis and the decrease of K^+ will cause the deactivation of cells [32]. Therefore, the release of K^+ was also studied to reflect the damage of cytomembrane. As can be seen in Fig. 4b, the concentration of K^+ increased from 0 mg/L to 1.19 mg/L in 60 min, which further verified the death of *E. coli* cells.

Then, the as-prepared materials were further tested to degrade RhB, MO, and MB dyes as depicted in Figs. 4c and d. An environmentally relevant concentration of 10 mg/L was used as the initial concentration for dyes [33]. The concentration of RhB kept unchanged in the blank experiment within 60 min, indicating RhB could not be degraded under the existence of visible light. The degradation efficiency was increased to 10%, 45% and 94% in the occurrence of pure Nb_2O_5, g-C_3N_4, and NO/CN, respectively. The kinetic data was well fitted with the first-order kinetic model ($\ln(C/C_0) = kt$) in Fig. S4 (Supporting information) [34], and the rate constant value (k_1) of NO/CN ($k_1 = 0.05\ min^{-1}$) was 5 and 50 times of Nb_2O_5 ($k_1 = 1 \times 10^{-3}\ min^{-1}$) and g-$C_3N_4$ ($k_1 = 1 \times 10^{-2}\ min^{-1}$), respectively. The enhanced RhB removal efficiency suggests the construction of heterojunction structure plays an essential effect in enhancing the photocatalytic capacities of materials [32]. Additionally, degradation of MO and MB was also tested to verify the photocatalytic activity (Fig. 4d). Compared to g-C_3N_4, the degradation efficiency increased from 0% to 15% for MO, and from 35% to 87% for MB, respectively, in the presence of NO/CN, further proving the superior photocatalytic performance of NO/CN towards various contaminants.

To explore the underlying reaction mechanism, different scavengers were added to the system to recognize the major radicals

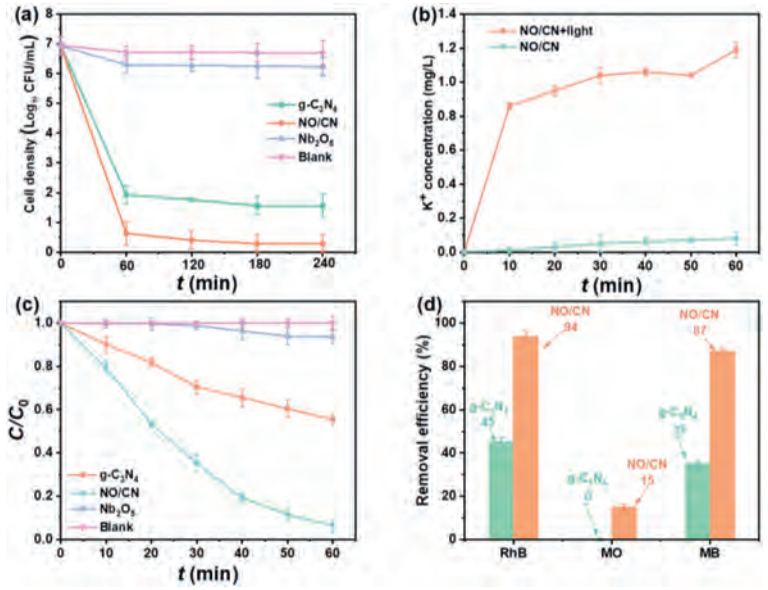

Fig. 4. (a) Photocatalytic performance of various materials on disinfection of *E. coli*. (b) Concentration of K^+ leakage of *E. coil* at different photocatalytic conditions. (c) The photocatalytic degradation of RhB by various materials. (d) The removal efficiency of RhB, MO, and MB by g-C_3N_4 and NO/CN. Experimental conditions: [*E. coli*] = 1.5 × 10^7 CFU/mL; [catalyst] = 0.5 g/L; [dyes] = 10 mg/L; pH 7 ± 0.2.

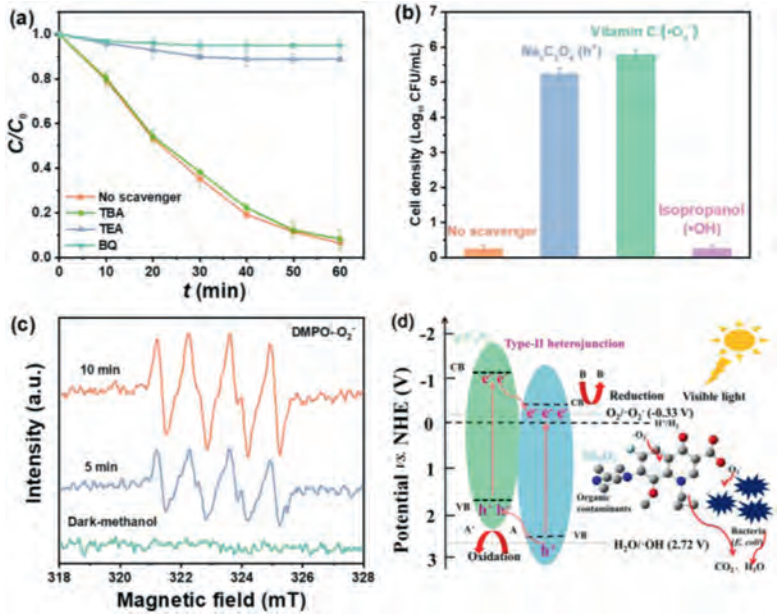

Fig. 5. Effects of various scavengers for photocatalytic removal of (a) RhB and (b) *E. coli* by NO/CN. (c) the ESR spectra of superoxide radical ($^{\bullet}O_2^-$) captured by DMPO on NO/CN dispersion in methanol aqueous under dark and after irradiation for 5 and 10 min. (d) The schematic diagram of mechanism for NO/CN. Experimental conditions: [*E. coli*] = 1.5 × 10^7 CFU/mL; [catalyst] = 0.5 g/L; [dyes] = 10 mg/L; [scavengers] = 1 mmol/L; pH 7 ± 0.2.

that contribute to the *E. coli* disinfection and dyes degradation by NO/CN composite. Accordingly, for dyes degradation, *tert*-butanol alcohol (TBA), triethanolamine (TEA), *p*-benzoquinone (BQ) were applied to quench the $^{\bullet}OH$, h^+ and $^{\bullet}O_2^-$ respectively [8,35–37] as described in Fig. 5a. The introduction of TBA had little effect on the degradation efficiency of RhB by NO/CN, which indicates $^{\bullet}OH$ plays a minor role during the photocatalytic removal of RhB. In addition, with the addition of TEA and BQ, the degradation of RhB was severely inhibited with the efficiency decreasing to 11% and 5%, respectively, illustrating that h^+ and $^{\bullet}O_2^-$ are the major ROSs for degrading pollutants. Additionally, in terms of *E. coli* disinfection, $Na_2C_2O_4$, isopropanol, and vitamin C (VC) were used to trap h^+, $^{\bullet}OH$ and $^{\bullet}O_2^-$ [38,39] respectively, as observed in Fig. 5b. The results were similar with dyes degradation, *i.e.*, isopropanol had sight impact on the *E. coli* disinfection by NO/CN material, suggesting that $^{\bullet}OH$ was not the dominate free radical during the photocatalytic disinfection of *E. coli*. The addition of $Na_2C_2O_4$ and VC inhibited extremely the disinfection of *E. coli* and disinfection efficiency was decreased to 1.8 and 1.2 log CFU/mL, respectively, indicating that h^+ and $^{\bullet}O_2^-$ played a significant role for inactivating *E. coli*. Furthermore, the ESR test was utilized to prove the formation of $^{\bullet}O_2^-$ during the photocatalytic process (Fig. 5c) [8]. In the dark condition, no $^{\bullet}O_2^-$ spectra were captured, while four distinct peaks of DMPO-$^{\bullet}O_2^-$ can be detected after 5 min visible light irradiation [40,41]. Meanwhile, the signal intensity of $^{\bullet}O_2^-$ became stronger when irradiation time was prolonged to 10 min, suggest-

ing the continuous generation of $^{\bullet}O_2^-$ radicals during the photocatalytic experiment. The ESR result was consistent with the radicals quenching experiments.

Based on the aforementioned results, the detail working mechanisms of NO/CN was depicted in Fig. 5d. g-C_3N_4 and Nb_2O_5 were activated easily and generated h^+ and e^- on the VB and CB, respectively, in the process of visible light illumination. g-C_3N_4, compared with Nb_2O_5, possesses higher Fermi level, leading photoinduced e^- of g-C_3N_4 (CB) readily migrate to the CB of Nb_2O_5, which enables e^- to accumulate in the CB of Nb_2O_5 and facilitate the formation of active species $^{\bullet}O_2^-$ [42]. Simultaneously, h^+ generated (VB) of Nb_2O_5 will migrate to the g-C_3N_4 (VB), thus forming a type-II heterojunction. As a consequence, the photoinduced e^- and h^+ were effectively separated and the recombination of e^- and h^+ pair were inhibited [43]. Hence, the inactivation performance and dyes removal efficiency were enhanced for composite materials under visible light. In this process, $^{\bullet}O_2^-$ and h^+ played the key role for inactivating *E. coli* and degrading pollutants. To be specific, the dissolved O_2 can capture e^- to form $^{\bullet}O_2^-$ in the CB of Nb_2O_5 and react with pollutants and bacteria. Similarly, the h^+ accumulated (VB) of g-C_3N_4 can react with pollutants and bacteria to generate the oxidized products as well. The following equations Eqs. 1–4 described the ROSs formation and the removal of contaminants process.

$$Nb_2O_5/g\text{-}C_3N_4 + h\nu \rightarrow h^+ + e^- \quad (1)$$

$$O_2 + e^- \rightarrow {}^{\bullet}O_2^- \quad (2)$$

$${}^{\bullet}O_2^- + \text{pollutants} \rightarrow \text{oxidizedproducts} \quad (3)$$

$$h^+ + \text{pollutants} \rightarrow \text{oxidizedproducts} \quad (4)$$

To sum up, a one-step heating method successfully synthesized the NO/CN composite material in this study. Characterization results confirmed the successful preparation of the heterojunction structure. Compared with pure g-C_3N_4, the NO/CN material exhibited excellent photocatalytic activities for *E. coli* activation and dyes removal under visible light irradiation. Besides, free radical quenching experiment and ESR test demonstrated that the main active substances were $^{\bullet}O_2^-$ and h^+ for removing pollutants and sterilization. The type II heterojunction structure of NO/CN facilitated the migration of photogenerated e^- and h^+ and hindered the recombination of photo-induced e^- and h^+ pairs, thereby enhancing the generation of ROSs and photocatalytic performance. Thus, the NO/CN composite seems a potential material towards the degradation of organic pollutants and bacteria in water treatment.

Declaration of competing interest

The authors declare that they have no known competing financial interests or personal relationships that could have appeared to influence the work reported in this paper.

Acknowledgments

Financial support from the Fundamental Research Funds for the Central Universities (No. 2019MS041) and Postdoctoral Science Foundation of China (No. 2021M690208) is highly acknowledged.

Supplementary materials

Supplementary material associated with this article can be found, in the online version, at doi:10.1016/j.cclet.2021.11.031.

References

[1] L. Zhao, J.H. Deng, P.Z. Sun, et al., Sci. Total Environ. 627 (2018) 1253–1263.
[2] P. Ganguly, C. Byrne, A. Breen, et al., Appl. Catal. B 225 (2018) 51–75.
[3] Q.B. Yuan, M.T. Guo, J. Yang, PLoS One 10 (2015) e0119403.
[4] N. Al-Jassim, M.I. Ansari, M. Harb, P.Y. Hong, Water Res. 73 (2015) 277–290.
[5] H. He, P. Zhou, K.K. Shimabuku, et al., Environ. Sci. Technol. 53 (2019) 2013–2026.
[6] D.M. Sievert, P. Ricks, J.R. Edwards, et al., Infect. Control Hosp. Epidemiol. 34 (2013) 1–14.
[7] F. Pan, Y. Yu, A.H. Xu, et al., J. Hazard. Mater. 340 (2017) 36–46.
[8] J. Ma, L. Chen, Y. Liu, et al., J. Hazard. Mater. 418 (2021) 126180.
[9] J. Duan, H.D. Ji, T.Y. Xu, et al., Chem. Eng. J. 406 (2021) 126752.
[10] Y. Li, X. Liu, L. Tan, et al., Adv. Funct. Mater. 29 (2019) 1900946.
[11] J. Zhou, X. Li, W. Sheng, et al., Appl. Catal. B 296 (2021) 120368.
[12] K. Zhang, D.Q. Li, H.Y. Cao, et al., Chin. Chem. Lett. 424 (2021) 130340.
[13] M.J. Calvete, G. Piccirillo, C.S. Vinagreiro, et al., Chem. Rev. 395 (2019) 63–85.
[14] C. Liu, D. Kong, P.C. Hsu, et al., Nat. Nanotechnol. 11 (2016) 1098–1104.
[15] Y. Wu, Q. Chen, S. Liu, et al., Chin. Chem. Lett. 30 (2019) 2186–2190.
[16] Q.Z. Huang, J.C. Wang, P.P. Wang, et al., Int. J. Hydrogen Energy 42 (2017) 6683–6694.
[17] S.W. Cao, J.X. Low, J.G. Yu, et al., Adv. Mater. 27 (2015) 2150–2176.
[18] S.W. Cao, J.Y. Guo, J. Phys. Chem. Lett. 5 (2014) 2101–2107.
[19] D. Huang, X. Yan, M. Yan, et al., ACS Appl. Mater. Interfaces 10 (2018) 21035–21055.
[20] S. Furukawa, T. Shishido, K. Teramura, et al., ACS Catal. 2 (2012) 175–179.
[21] J.Q. Yan, G.J. Wu, N.J. Guan, et al., Appl. Catal. B (2014) 280–288 152-153.
[22] K.T.G. Carvalho, A.E. Nogueira, O.F. Lopes, et al., Ceram. Int. 43 (2017) 3521–3530.
[23] Y.P. Xing, X.K. Wang, S.H. Hao, et al., Chin. Chem. Lett. 32 (2021) 13–20.
[24] P.F. Xia, S.W. Cao, B.C. Zhu, et al., Angew. Chem. Int. Ed. 59 (2020) 2–10.
[25] Y.Z. Hong, C.S. Li, G.Y. Zhang, et al., Chem. Eng. J. 299 (2016) 74–84.
[26] X.C. Wang, K. Maeda, A. Thomas, et al., Nat. Mater. 8 (2009) 76–80.
[27] T.T. Zhu, Y.H. Song, H.Y. Ji, et al., Chem. Eng. J. 271 (2015) 96–105.
[28] A.P. Dementjev, A. de Graaf, M.C.M. van de Sanden, et al., Diamond Relat. Mater. 9 (2000) 1904–1907.
[29] Y. Zang, L. Li, X. Li, et al., Chem. Eng. J. 246 (2014) 277–286.
[30] J.Q. Yan, G.J. Wu, N.J. Guan, et al., Appl. Catal. B (2014) 280–288 152-153.
[31] D.L. Wood, J. Tauc, Phys. Rev. B 5 (1972) 3144–3151.
[32] H. Shi, G. Huang, D. Xia, et al., J. Phys. Chem. B 119 (2015) 3104–3111.
[33] Y. Li, X.N. Zheng, J. Yang, Z.H. Zhao, S.H. Cui, J. Taiwan Inst. Chem. Eng. 119 (2021) 213–223.
[34] J. Duan, H.D. Ji, X. Zhao, et al., Chem. Eng. J. 393 (2020) 124692.
[35] M.Y. Wang, H. Wang, Y.H. Ren, et al., Nanomaterials 8 (2018) 427–439.
[36] T.T. Zhu, Y.H. Song, H.Y. Ji, et al., Chem. Eng. J. 271 (2015) 96–105.
[37] B.Y. Peng, S.S. Zhang, S.Y. Yang, et al., Mater. Res. Bull. 56 (2014) 19–24.
[38] L.Q. Ye, J.Y. Liu, C.Q. Gong, et al., ACS Catal. 2 (2012) 1677–1683.
[39] J. Guo, H. Shi, X. Huang, et al., J. Colloid Interface Sci. 515 (2018) 10–17.
[40] X.J. Bai, L. Wang, R.L. Zong, et al., J. Phys. Chem. C 117 (2013) 9952–9961.
[41] X.Y. Xiao, J. Jiang, L.Z. Zhang, et al., Appl. Catal. B (2013) 487–493 142-143.
[42] K. Gelderman, L. Lee, S. Donne, J. Chem. Educ. 84 (2007) 685–688.
[43] C. Zhao, M. Pelaez, X.D. Duan, et al., Appl. Catal. B 134-135 (2013) 83–92.